Environ. Sci. Technol. **2007**, *41,* 5747−5755

Disentangling Oil Weathering Using GC×GC. 2. Mass Transfer Calculations

J. SAMUEL AREY,[†] ROBERT K. NELSON,[‡] DESIREE L. PLATA,[‡] AND CHRISTOPHER M. REDDY[‡]

Laboratory of Biochemistry and Computational Chemistry, Swiss Federal Institute of Technology, Lausanne, Switzerland, and Department of Marine Chemistry and Geochemistry, Woods Hole Oceanographic Institution, Woods Hole, Massachusetts

Hydrocarbon mass transfers to the atmosphere and water column drive the early weathering of oil spills and also control the chemical exposures of many coastal wildlife species. However, in the field, mass transfer rates of individual hydrocarbons to air and water are often uncertain. In the Part 1 companion to this paper, we used comprehensive two-dimensional gas chromatography (GC×GC) to identify distinct signatures of evaporation and dissolution encoded in the compositional evolution of weathered oils. In Part 2, we further investigate patterns of mass removal in GC×GC chromatograms using a mass transfer model. The model was tailored to conditions at a contaminated beach on Buzzards Bay, MA, after the 2003 *Bouchard 120* oil spill. The model was applied to all resolved hydrocarbon compounds in the $C_{11}-C_{24}$ boiling range, based on their GC×GC-estimated vapor pressures and aqueous solubilities. With no fitted parameters, the model successfully predicted GC×GC chromatogram patterns of mass removal associated with evaporation, water-washing, and diffusion-limited transport. This enabled a critical field evaluation of the mass transfer model and also allowed mass apportionment estimates of hundreds of individual hydrocarbon compounds to air and water. Ultimately, this method should improve assessments of wildlife exposures to oil spill hydrocarbons.

Introduction

On April 27, 2003, the single-hulled barge, *Bouchard 120*, struck a submerged ledge in Buzzards Bay, Massachusetts, and spilled approximately 370 000 L of heavy fuel oil (*1*). The *Bouchard 120* carried a No. 6 fuel oil, a heavy oil amended with a lighter petroleum product (*2*). The resulting mixture resembled a fresh crude oil; it consisted of hydrocarbon compounds having an *n*-alkane boiling point range of *n*-C_{10} to greater than *n*-C_{45} (*3*). Within days, wind and waves pushed the oil slick onto 150 km of Buzzards Bay shoreline (*2*). Using comprehensive two-dimensional gas chromatography (GC×GC), Nelson et al. examined two samples of weathered *Bouchard 120* oil at a heavily contaminated cobble beach, Nyes Neck (*3*). Within two weeks of the spill, the oil had hardened into a viscous coating onto the golf-ball-sized Nyes Neck cobbles and showed signs of slight weathering. By comparison, a sample collected at 6 months exhibited significant compositional evolution (*3*). As explained in our companion paper (*4*), conventional weathering diagnoses are unlikely to differentiate the effects of evaporation, water-washing, and degradation of these samples. In the following report, we expand on the Nelson et al. study by investigating 13 weathered samples collected over the course of weathering during the first 16 weeks after the *Bouchard 120* spill. Moreover we combine a novel, GC×GC-based data analysis technique (*4*) together with mass transfer modeling to rigorously differentiate evaporation and dissolution experienced by oil at Nyes Neck.

Several existing models describe oil compositional changes caused by weathering. Many years ago, Mackay and coworkers developed robust expressions for evaporation and dissolution rates of individual compounds from oil (*5*, *6*). These authors assumed that evaporation and dissolution rates are driven by partitioning disequilibrium between the oil phase and adjacent (air, water) phase and restrained by a "mass transfer coefficient", characterized by interfacial and environmental conditions (*7*, *8*). The resulting expressions have been tested in subsequent studies (*9*−*12*), and these and related approaches are employed in composite oil spill fate models (*13*, *14*). In spite of this, attention is usually focused on biodegradation (*15*), and scientists rarely publish expected mass loss rates due to evaporation or dissolution in oil weathering field studies. Using data from controlled water-washing experiments of *Exxon Valdez* oil, Short and Heintz empirically fitted the aggregate (physical plus biological) mass removal kinetics of 14 polycyclic aromatic hydrocarbon (PAH) groups using a first-order loss rate model (*16*). The model assumed that each PAH group had a unique weathering response factor held constant across all samples. Each sample was assigned a unique weathering exposure coefficient which reflected the integrated weathering time, thus allowing the model to explain differences between samples. The values of weathering coefficients and response factors were constrained such that their linear combination resulted in the best fit of the observed mass losses of all PAH groups across all samples. The model usefully described PAH weathering patterns in field samples of several spills (*16*, *17*), but it did not identify the relative importances of underlying weathering mechanisms.

In this study we conducted a mass transfer analysis of evaporation and water-washing for several field samples from the *Bouchard 120* oil spill. We hypothesized that by applying physical models of mass transfer to GC×GC chromatograms of the weathered oil, we could distinguish evaporation and water-washing from other weathering effects, across the $C_{11}-C_{24}$ boiling range compositional space. To test this hypothesis, we compared model predictions with the observed weathering of heavy fuel oil on Nyes Neck beach during the first 16 weeks after the *Bouchard 120* spill. None of the model parameters were fitted to observed compositional changes in the samples.

Materials and Methods

Sample Collection and Preparation, GC×GC Analysis. Several oil-covered cobbles (2−4 cm diameter) were collected from Nyes Neck beach in North Falmouth, MA, over a 122 day period after the *Bouchard 120* spill (April 27−Aug 26). Samples were gathered from the "surf zone", which was regularly exposed to both wind and water, and also from the high beach where surf rarely reached ("dry zone"). Twenty-

* Corresponding author phone: +41 21 693 0322; fax: +41 21 693 0320; e-mail: arey@alum.mit.edu.
[†] Swiss Federal Institute of Technology.
[‡] Woods Hole Oceanographic Institution.

10.1021/es070006p CCC: $37.00
Published on Web 07/14/2007

four cobbles were analyzed for total soluble extractable material (TSEM) as follows. Duplicate extractions by 15-minute sonication in dichloromethane/methanol (90:10) were performed. The combined fractions were washed with deionized water, collected, concentrated by rotary evaporation, and dried over activated sodium sulfate. To determine the TSEM mass, which included asphaltenes, a fraction of the sample extract was dried and weighed. The TSEM was considered equivalent to the total oil loading on each cobble. In addition to TSEM measurements, 13 samples from the first 114 days of weathering (May 6−Aug 18) were extracted using a slightly different protocol and analyzed by GC×GC (*4*). Separately, asphaltene content was determined by measuring the mass of fresh oil material insoluble in heptane.

Data Analysis. To compare weathering model predictions to GC×GC chromatograms of real weathered oil, several GC×GC data analysis methods were first developed. These methods are fully detailed in a previous work (*18*, *19*) and in our companion paper (*4*). Briefly, chromatogram retention times were converted into estimates of hydrocarbon component vapor pressures, aqueous solubilities, enthalpies of vaporization, and molecular weights for the C_{11}−C_{24} boiling range of GC×GC chromatograms (*4*, *18*, *19*). Using a finite element method, GC×GC chromatograms were discretized into sub-regions (cells) such that each cell reflected a unique hydrocarbon volatility and aqueous solubility. For each cell *i*, we evaluated the ln-transformed mass fraction remaining, $\ln[M_i(t)/M_i(t_0)]$, of the weathered samples (time *t*) with respect to the fresh oil (time t_0). We refer to the resulting array of cells as a "mass loss table" or MLT (*4*). The rows and columns of the MLT vary systematically in volatilities and aqueous solubilities of analyzed hydrocarbons, respectively. Consequently, the MLT directly diagnoses the effects of volatilization and dissolution on the entire oil mixture (*4*). Each chromatogram was normalized to C_{30} 17α,21β-hopane, which was conserved in these samples (*4*).

Mass Transfer Model. A mass transfer model was developed to predict the time-dependent compositional changes of *Bouchard 120* oil due to evaporation and aqueous dissolution:

$$\frac{dM_i}{dt} = \left.\frac{dM_i}{dt}\right|_{evap} + \left.\frac{dM_i}{dt}\right|_{diss} \quad (1)$$

where M_i is the mass of compound *i* in the oil, and *t* is time. The model formulation reflected contamination conditions of surface cobbles at Nyes Neck beach. The heavy oil had painted the 1−10 cm diameter Nyes Neck cobbles with a coat of highly viscous residue. We therefore assumed that the mass removal rate of oil compounds was controlled by diffusion out of the oil phase; partitioning into the adjoining phase (air or water); and finally diffusion through a thin layer of the adjoining phase (air or water). These processes are described by the one-dimensional "two-film" mass transfer model (*8*, *20*), expressed as:

$$\left.\frac{dM_i}{dt}\right|_{evap} = -\frac{\frac{M_i}{\delta_{oil}}}{\left(\frac{\delta_{oil}}{D_{i,oil}} + \frac{\delta_{air}}{D_{i,air}K_{i,a/o}}\right)} \quad (2)$$

$$\left.\frac{dM_i}{dt}\right|_{diss} = -\frac{\frac{M_i}{\delta_{oil}}}{\left(\frac{\delta_{oil}}{D_{i,oil}} + \frac{\delta_{water}}{D_{i,water}K_{i,w/o}}\right)} \quad (3)$$

where δ_j is the film thickness of phase *j*, $D_{i,j}$ is the diffusivity of compound *i* in the indicated phase, and $K_{i,j/k}$ is the partition coefficient of compound *i* between phases *j* and *k*. Equation 3 is equivalent to the expression employed by Southworth and co-workers (*21*, *22*) for aqueous dissolution kinetics of compounds from a resting oil film. The "mass transfer coefficients" in their works are interpreted here as diffusive velocities, $D_{i,j}/\delta_j$, across a thin film layer (*20*). In most previous models of oil dissolution or evaporation kinetics (*5*−*7*, *9*−*12*, *23*), diffusion within the oil phase was neglected. We explicitly included oil phase diffusion because the *Bouchard 120* is a very viscous oil in which we expected relatively low diffusion rates. We anticipated that a detailed mass transfer analysis, combined with the resolving power of GC×GC, may elucidate evidence of oil phase diffusion-limited mass transfer. Employing eqs 2 and 3, eq 1 can be integrated for $M_i(t)$ from initial time t_0 (the day of the spill, April 27) to time *t*, assuming all parameters are constant:

$$\ln\left(\frac{M_i(t)}{M_i(t_0)}\right) = -\frac{(t-t_0)}{\delta_{oil}\left(\frac{\delta_{oil}}{D_{i,oil}} + \frac{\delta_{air}}{D_{i,air}K_{i,a/o}}\right)} - \frac{(t-t_0)}{\delta_{oil}\left(\frac{\delta_{oil}}{D_{i,oil}} + \frac{\delta_{water}}{D_{i,water}K_{i,w/o}}\right)} \quad (4)$$

In the case where solute diffusion through the oil phase is unimportant (i.e., $D_{i,oil}/\delta_{oil} \gg K_{i,a/o}D_{i,air}/\delta_{air}$ and $D_{i,oil}/\delta_{oil} \gg K_{i,w/o}D_{i,water}/\delta_{water}$), eq 4 simplifies to

$$\ln\left(\frac{M_i(t)}{M_i(t_0)}\right) = -\frac{D_{i,air}K_{i,a/o}(t-t_0)}{\delta_{oil}\delta_{air}} - \frac{D_{i,water}K_{i,w/o}(t-t_0)}{\delta_{oil}\delta_{water}} \quad (5)$$

The two right-hand-side terms of eq 5 are similar to expressions developed by Mackay and others to describe evaporation and dissolution rates from an oil phase (*5*−*7*, *9*−*11*, *23*). Equation 4 differs from eq 5 only in that diffusion through oil contributes an additional mass transfer resistance term.

Both eqs 4 and 5 were used to predict evaporation and dissolution kinetics of residual *Bouchard 120* oil at Nyes Neck beach. Within the approximations of either eq 4 or eq 5, the characteristic rate constants of evaporation and dissolution are additive for individual solutes:

$$\ln\left(\frac{M_i(t)}{M_i(t_0)}\right) = -[k_{i,evap} + k_{i,diss}](t-t_0) \quad (6)$$

Hence, to the extent that the evaporation, dissolution, biodegradation, and photodegradation of individual compounds obey first-order kinetics, $\ln[M_i(t)/M_i(t_0)]$ is the appropriate quantity to analyze for differentiating weathering effects. This assumption agrees with previous observations: Short and Heintz observed first-order loss rate kinetics of PAHs in a large set of weathered *Exxon Valdez* samples (*16*). Some input parameters to eqs 4−5 were time-dependent. Hence both models (eq 4 and eq 5) were evaluated as a sum of integrated short time periods:

$$\ln\left(\frac{M_i(t_N)}{M_i(t_0)}\right) = \ln\left(\frac{M_i(t_1)}{M_i(t_0)}\right) + \ln\left(\frac{M_i(t_2)}{M_i(t_1)}\right) + \ln\left(\frac{M_i(t_3)}{M_i(t_2)}\right)\ldots$$
$$= -[k_{i,evap}^{0\to1} + k_{i,diss}^{0\to1}](t_1-t_0) - [k_{i,evap}^{1\to2} + k_{i,diss}^{1\to2}](t_2-t_1) - [k_{i,evap}^{2\to3} + k_{i,diss}^{2\to3}](t_3-t_2)\ldots \quad (7)$$

where each $k_{i,evap}^{n\to n+1}$ and $k_{i,diss}^{n\to n+1}$ was calculated using representative input parameters (Table 1) assumed constant over the time period t_n to t_{n+1}. Dry zone and surf zone samples were differentiated in the model. In simulations of the dry

TABLE 1. Weathering Simulation Input Parameters[a]

chemical and environmental parameters	symbol	value
air boundary film thickness	δ_{air}	0.2 cm
water boundary film thickness	δ_{water}	0.02 cm
initial oil film thickness	$\delta_{oil}(t_0)$	0.0035 cm
initial fraction of asphaltene mass in the oil	$M_{asphalt}(t_0)/M_{total}(t_0)$	0.21
Setchenow solubility factor for seawater salinity	K_{salt}	1.3
oil molar volume	V_{oil}	0.4 L/mol

[a] Some model inputs (T, $D_{i,air}$, $D_{i,water}$, $D_{i,oil}$, $K_{i,a/o}$, $K_{i,w/o}$, $\Delta_{vap}H_i$) are not listed, since they varied with respect to chemical identity (GC×GC retention index) or time (t), as explained in the text.

zone, only evaporation affected the samples. In surf zone simulations, samples were evaporated for 12 h and water-washed for 12 h each day.

The partition coefficients, $K_{i,a/o}$ and $K_{i,w/o}$, were estimated using Raoult's law:

$$K_{i,a/o} = \frac{P_i^L V_{oil}}{RT} \quad (8)$$

$$K_{i,w/o} = \frac{C_i^{w,sat} V_{oil}}{K_{salt}} \quad (9)$$

where P_i^L is the hypothetical pure component liquid vapor pressure of solute i, $C_i^{w,sat}$ is the hypothetical liquid aqueous solubility of solute i, K_{salt} is a factor (est. ~1.3) accounting for the effect of seawater salt on hydrocarbon solubility (*20*), V_{oil} is the molar volume of the oil mixture, R is the molar gas constant, and T is oil temperature. Since P_i^L is strongly dependent on temperature, we calculated $P_i^L(T)$ as

$$P_i^L(T) = P_i^L(T_{ref}) \exp\left[-\frac{\Delta_{vap}H_i}{R}\left(\frac{1}{T} - \frac{1}{T_{ref}}\right)\right] \quad (10)$$

where T_{ref} is a reference temperature (298 K) and $\Delta_{vap}H_i$ is the enthalpy of vaporization for solute i. Aqueous solubility was assumed constant with T. The formulations given by eqs 8−10 were very useful in conjunction with GC×GC, because estimates of $P_i^L(T_{ref})$, $C_i^{w,sat}$, and $\Delta_{vap}H_i$ were directly mapped onto the GC×GC chromatogram for hydrocarbon solutes (*4*, *18*, *19*).

The environmental parameters, T, δ_{air}, δ_{water}, δ_{oil}, and V_{oil}, and hydrocarbon solute parameters, $D_{i,air}$, and $D_{i,water}$, were estimated as follows (see Supporting Information for a summary). Mackay and Matsugu (*7*) observed that a resting oil exposed to solar radiation (at 43° N latitude and during summer) would reach temperatures of 10−20 °C above ambient temperature (~25 °C) near midday. Based on this consideration and using measured ocean temperature (T_{water}) and air temperature (T_{air}) data taken at 20 min intervals (see Supporting Information) from the nearby Martha's Vineyard Coastal Observatory (42° N latitude), we estimated the residual oil temperature (T) on Nyes Neck beach during the period from April 27 to August 18, 2003. For surf zone samples, we approximated $T = T_{water}$. For dry zone samples, we approximated $T = T_{air} + I/70$, where I = measured solar radiation (W/m^2); this resulted in a daily maximum of $T \approx T_{air} + 14$ °C for a sunny summer day. Model values for δ_{air} (0.2 cm) and δ_{water} (0.02 cm) reflected typical environmental mass transfer rates consistent with many previous studies, including studies not involving oil (*20*). Average oil thicknesses on several beach cobbles were estimated based on the rock surface area and TSEM oil mass, assuming a uniform layer of oil on the cobble and an oil density of 0.99 g/cm^3. Based on results from TSEM measurements, we assumed that all samples had an initial oil loading of $\delta_{oil}(t_0) = 0.0035$ cm for the purposes of simulations. To account for cumulative mass hydrocarbon loss, the δ_{oil} parameter was recalculated at every time step such that $\delta_{oil}(t) = \delta_{oil}(t_0) \times (M_{total}(t)/M_{total}(t_0))$, where $M_{total}(t)$ is given by the sum of $M_i(t)$ for all solutes i, including asphaltenes (where $M_{asphalt}(t_0)/M_{total}(t_0) = 0.21$, based on asphaltene measurement of the original oil). Asphaltenes contributed significantly to oil mass but were assumed impervious to mass transfer. V_{oil} was estimated as 0.4 L/mol, based on the molecular weight distribution of the early weathered material (*3*) and a measured mixture density of 0.99 g/cm^3. Model results were not sensitive to expected changes in V_{oil}, thus V_{oil} was assumed constant over time. Solute $D_{i,air}$ and $D_{i,water}$ values were estimated from molecular weight (*20*) and were assumed independent of T. A temperature correction was not applied to diffusivities in air and water because this effect was considered small compared to other sources of variability and uncertainty. Solute molecular weight estimates were mapped directly onto GC×GC chromatograms (*4*) so that $D_{i,air}$ and $D_{i,water}$ estimates were tailored to individual solutes across the C_{11}−C_{24} boiling point range.

Solute $D_{i,oil}$ values were estimated using the Stokes−Einstein relation (*20*):

$$D_{i,oil} = \frac{k_B T}{6\pi\eta_{oil} r_i} \quad (11)$$

where η_{oil} is the dynamic viscosity of the oil, r_i is the solute radius (we assumed r_i ~5 Å), and k_B is the Boltzmann constant. Equation 11 is theoretically grounded, but its applicability to hydrocarbons in highly viscous weathered oils (very large η_{oil}) is unclear. In dissolution experiments of phenols, anilines, and aromatic hydrocarbon solutes from several resting oils, Herbes et al. found that the oil-side mass transfer coefficient was proportional to $\eta_{oil}^{-1.23}$ (*22*), in contrast to the proportionality with $\eta_{oil}^{-1.0}$ suggested by eq 11. By comparison, Kowert and Dang found dioxygen diffusion coefficients proportional to $\eta_{oil}^{-0.56}$ for several alkane solvents (*24*), consistent with the expectation that eq 11 worsens as solute size decreases relative to solvent molecules. Neither of these experiments evaluated extremely high viscosity mixtures such as an evaporatively weathered heavy oil (*13*). Equation 11 was therefore considered a very approximate estimate of diffusivity in oil. Based on viscosity measurements (Triton Analytics Corp.) of the fresh (unweathered) oil, we found

$$\log_{10}(\eta_{oil}) = -0.0450T + 14.787 \quad r^2 = 0.9997 \quad (12)$$

where T is in K and η_{oil} is in Pa·s. Note that fitted coefficients to eq 12 are unique to individual oils (*25*). We also applied the Mackay viscosity correction for a heavy oil (*26*)

$$\eta_{oil}(weathered) = \eta_{oil}(fresh)e^{10(fraction\ evaporated)} \quad (13)$$

to account for increased viscosity due to the evaporation of lighter oil components. The prefactor "10" in the exponent of eq 13 was considered appropriate for a heavy oil (*26*). Using Martha's Vineyard Coastal Observatory T conditions as inputs to eqs 12 and 13, we calculated the weathered oil viscosity in the dry zone and surf zone at each time step during the 2003 weathering period. Then we estimated $D_{i,oil}$ using eq 11 throughout the simulation.

Results and Discussion

Predicted and Observed Aggregate Rates of Oil Removal. Simulated mass transfer accounted for most of the observed

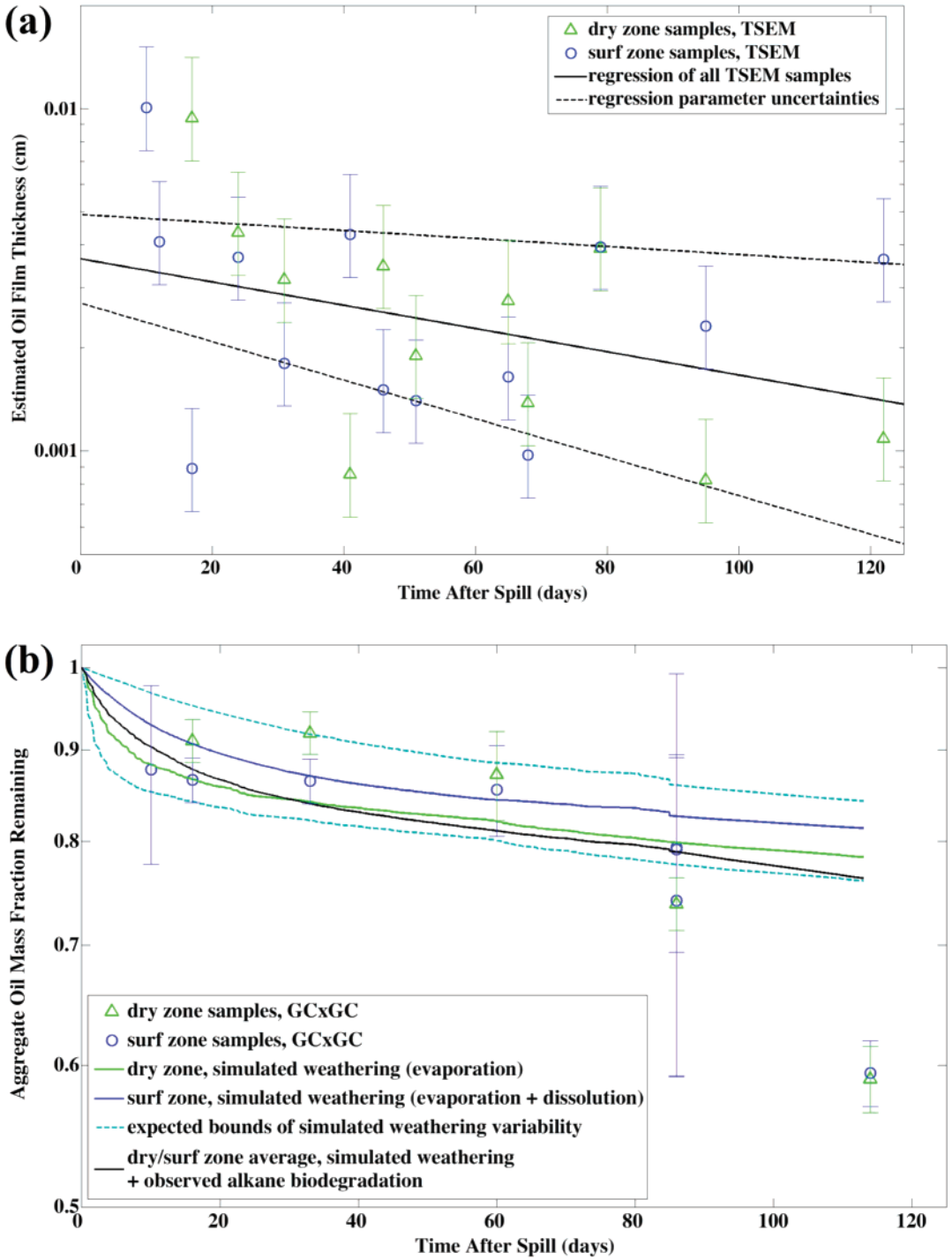

FIGURE 1. Measured and simulated aggregate mass loss rate on Nyes Neck cobbles. (a) The calculated slope and intercept from a regression of TSEM (total soluble extractable material) trends suggested an aggregate mass loss rate of 0.008 ± 0.006 day^{-1} and initial oil thickness of 0.0018−0.0070 cm (0.0035 cm average). Sample oil thickness uncertainties reflect nonuniform loadings on individual cobbles. (b) The hopane-normalized mass loss trends deduced from GC×GC-analyzed sample compositions gave a better aggregate weathering rate estimate (0.0037 ± 0.0003 day^{-1}). Four surf zone samples exhibited unusually high mass loss uncertainties due to an unanticipated leak in GC×GC column fittings (*4*).

aggregate mass loss from oiled cobbles at Nyes Neck during initial months of weathering. Observed oil loadings were highly variable, but average loading decreased steadily over the summer of 2003 (Figure 1). Assuming that aggregate oil mass followed first-order loss rate kinetics

$$M_{total}(t) = M_{total}(t_0)\ \exp[-k_{overall}(t - t_0)] \qquad (14)$$

we initially estimated $k_{overall} = 0.008 \pm 0.006$ day^{-1} by linear regression of the TSEM on 24 different cobbles (Figure 1a). However the TSEM-based loss rate estimate was highly uncertain; within a 95% confidence interval, observed oil thicknesses varied by ×4 with respect to the regression. In the 13 GC×GC-analyzed samples, trends in the hopane-normalized total mass (including asphaltenes) suggested $k_{overall} = 0.0037 \pm 0.0003$ day^{-1}, thus improving the loss rate estimate (Figure 1b). This corresponds to an oil mass half-life of about 200 days, comparable to the estimated initial weathering half-life of 100 days found for thin films of *Exxon*

Valdez oil exposed to freely circulating air and water (*27*). Notably, simulated evaporation and dissolution of the aggregate oil mass did not follow first-order loss rate kinetics (Figure 1b). Although individual compounds follow a first-order loss rate (eqs 4 and 5), the aggregate mixture does not necessarily display a first-order loss rate due to mass transfer (*28*). However, in order to compare early weathering mass transfer rates with other processes, we roughly estimated first-order loss rate constants of $k_{evap} \approx 0.0019 \pm 0.0005$ day^{-1} and $k_{diss} \approx 0.0005 \pm 0.0001$ day^{-1} for the aggregate mixture, based on the simulated mass transfer to air and water during the first 114 days and assuming an initial oil loading distribution of 0.0018−0.0070 cm (Figure 1b). By comparison, measured *n*-alkane losses accounted for about $k_{degradation} \approx 0.0005 \pm 0.0001$ day^{-1} of the aggregate mixture in GC×GC-analyzed samples (*4*). Hence evaporation and dissolution of the aggregate mixture plus biodegradation of *n*-alkanes together accounted for $k_{removal} \approx 0.0029 \pm 0.0005$ day^{-1}, or about 80% of the observed aggregate mass loss rate of 0.0037 $\pm$ 0.0003 day^{-1}. Therefore the remaining mass losses, which mostly occurred in late summer (Figure 1b), were attributed to degradation of compounds other than *n*-alkanes.

Predicted and Observed Evaporation and Dissolution Signatures. Mass transfer model predictions were consistent with the predominant weathering trends observed in Nyes Neck oil samples (Figure 2), despite modeling simplifications. To allow robust quantitative comparisons between the model and weathering observations, we reduced GC×GC compositional data to 149 MLT cells that formed an orthogonal basis in the dimensions of volatility and solubility, for each oil sample (*4*). Mass transfer calculations successfully captured 73% of the observed variability of 1937 total independent measured compositional changes (149 MLT cells in each of 13 weathered samples) during the first 16 weeks of oil weathering. The root-mean-squared-error (rmse) of the predicted MLTs was 0.34 in the log $[M_i(t)/M_i(t_0)]$ for a given cell, *i*. For example if 80% mass loss was observed for a particular cell *i*, the model typically predicted a mass loss ranging from 60% to 90% for this cell.

Simulations correctly predicted a prominent evaporation front in all samples. We defined an "evaporation front" as the region delineating the systematic progression of mass removal along the dimension of solute vapor pressure (*4*). In both observed and simulated samples, the evaporation front in the dry zone progressed significantly faster than in the surf zone. In simulations, this was due to increased temperatures and increased atmospheric exposure of the dry zone relative to the surf zone. In all 13 samples, the calculated and observed positions of the evaporation front agreed to within about one unit in the log vapor pressure. The discrepancies between simulated and observed positions of the evaporation front are partly explainable by known variability in the initial oil loadings among samples. In simulations, the initial oil thickness ($\delta_{oil}(t_0) = 0.0035$ cm) was assumed identical in all samples, but in reality, sampled cobbles experienced about 4-fold variability in oil thickness at any given stage of weathering (Figure 1a). In additional simulations (not shown), we found that increasing or decreasing the initial model oil thickness by a factor of 4 shifted the simulated evaporation front position by 0.6−1.0 in the log vapor pressure, depending on the stage of weathering. This is consistent with the observed variability, of about 1.0 in the log vapor pressure, in the position of the evaporation front among the 3 day 86 surf zone samples (Figure 2i, j, and k). Importantly, this variability explains why the observed positions of some evaporation fronts are slightly early or late compared to simulations. Previous studies report significant physical weathering heterogeneity of crude or heavy oils among samples experiencing similar environmental conditions (*15*, *29*−*31*). Here we emphasize a mechanistic explanation of physical weathering heterogeneity: differences in the initial thickness of a heavy oil result in different weathering trajectories in the environment (*17*), as reflected by eqs 4 and 5.

Simulations accurately predicted observed rates of oil dissolution. Excluding the two earliest samples (day 10 and day 16), all surf zone samples showed clear evidence of a dissolution front (*4*). Consistent with these observations, simulated dissolution did not strongly influence oil composition until after the first two weeks. The locations of the observed and simulated dissolution fronts were consistent to within about 0.5 log solubility units across all surf zone samples. In the dry zone, two samples (day 33 and day 114) showed losses of water-soluble compounds not explainable by evaporation. For the late summer sample (day 114), these dry zone losses are likely explainable by biodegradation and photodegradation (*4*). In other words, observations and model calculations indicate that many hydrocarbons experienced different fates in the surf zone versus the dry zone.

Simulated effects of oil phase diffusion were consistent with observations in some samples but not others. According to eq 4, oil diffusion-limited transport should be most important for volatile hydrocarbons (high $K_{i,a/o}$) in high oil loadings (large δ_{oil}) at low temperatures (decreased T increases η_{oil} and hence decreases $D_{i,oil}$). Thus the model predicted that oil diffusion-limited transport mostly affects light hydrocarbons immediately after the spill, in the cool spring surf zone conditions. The simulated oil diffusion signature is evident as a broadening of the mass removal front (Figure 3). According to simulations, oil phase diffusion-limited transport was significant until day 33 in the dry zone and until day 60 in the surf zone. In agreement with simulation, the two earliest dry zone samples (days 16, 33) exhibited broadened mass loss signatures, consistent with oil diffusion-limited transport. However the model overpredicted the oil-side diffusion resistance in the day 10 and day 16 surf zone samples. Additionally, the samples suggest that oil-side diffusion resistance affects mass transfer until day 86 in the surf zone, and this was underpredicted by the model. These inaccuracies are unsurprising given the variability in oil loadings and the rudimentary assumptions that were used to parameterize $D_{i,oil}$. Moreover, oil diffusion-limited transport contributed only a second-order correction to mass transfer calculations. Hence it is reasonable to ask whether the effort of parameterizing eq 4 was worthwhile compared to using the simpler expression, eq 5. Equation 5 predicted the evaporation and dissolution rates of affected compounds with useful accuracy (not shown). However, eq 4 can aid future investigators in deciding whether oil diffusion-limited transport is important. In hypothetical cases where high loadings of heavy oils are deposited in cold conditions, oil diffusion-limited transport may be important. Diffusion partly controls the fate of buried oil in sediments (*31*, *32*). Some phenomena protect oils from weathering for long periods of time, such as the formation of stable mousses or development of a viscous skin at the oil−air interface (*6*, *13*, *33*−*35*), and these could be analyzed in terms of diffusion-limited transport.

Reinterpretation of the Short and Heintz Weathering Rate Parameter. Analysis of the Short and Heintz empirical weathering model (*16*) provided additional validation of the mass transfer expressions used here. Short and Heintz found first-order loss rate kinetics of several PAHs in a large set of water-washed oil samples

$$\ln\left(\frac{M_i(t)}{M_i(t_0)}\right) = -k_i w = -k_i\left(\frac{\mathrm{d}w}{\mathrm{d}t}\right)(t - t_0) \qquad (15)$$

where w is a weathering exposure parameter, $\mathrm{d}w/\mathrm{d}t$ is a "weathering rate", found to be approximately constant with

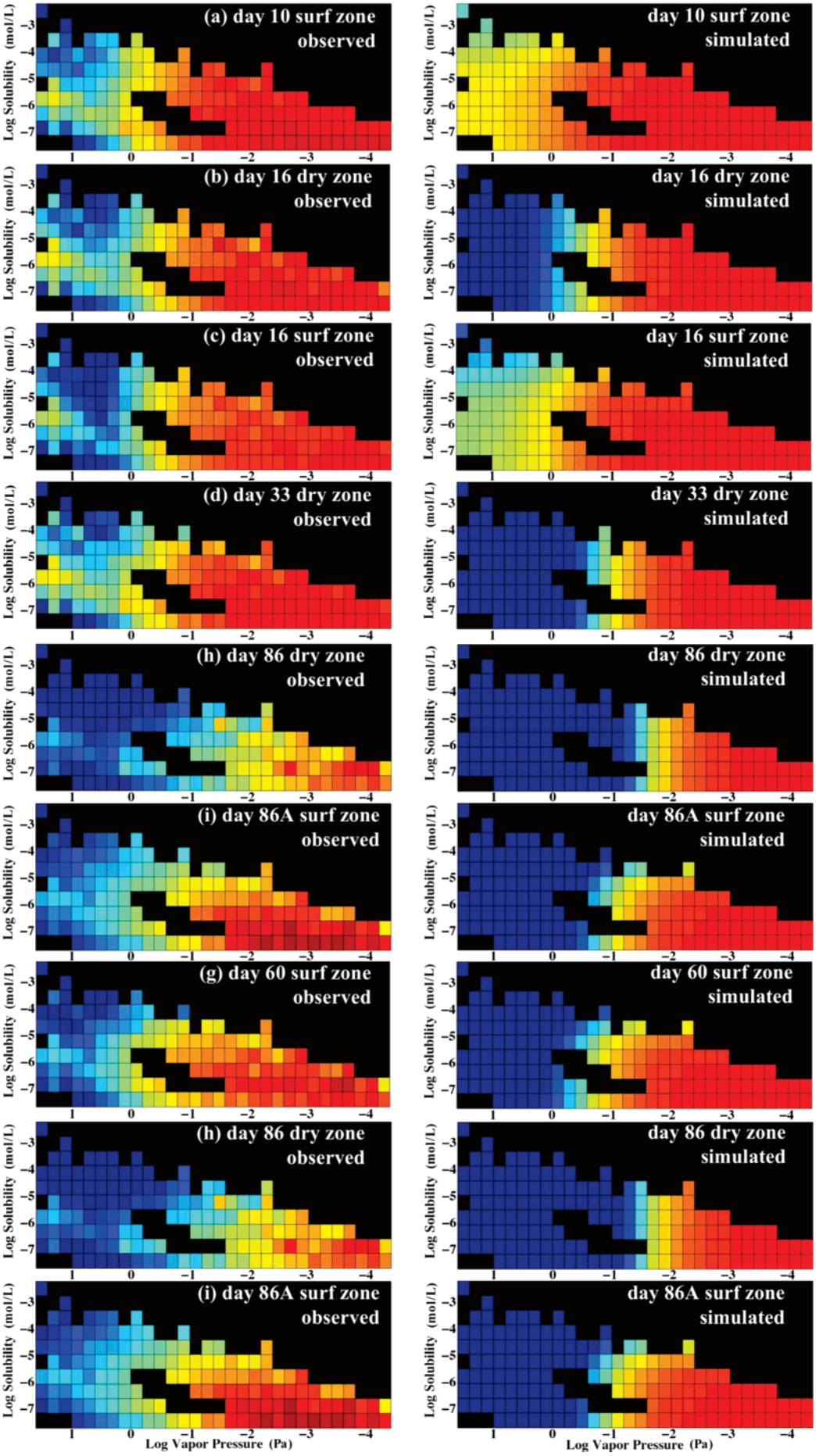
(a) day 10 surf zone observed
day 10 surf zone simulated
(b) day 16 dry zone observed
day 16 dry zone simulated
(c) day 16 surf zone observed
day 16 surf zone simulated
(d) day 33 dry zone observed
day 33 dry zone simulated
(h) day 86 dry zone observed
day 86 dry zone simulated
(i) day 86A surf zone observed
day 86A surf zone simulated
(g) day 60 surf zone observed
day 60 surf zone simulated
(h) day 86 dry zone observed
day 86 dry zone simulated
(i) day 86A surf zone observed
day 86A surf zone simulated
Log Solubility (mol/L)
Log Vapor Pressure (Pa)

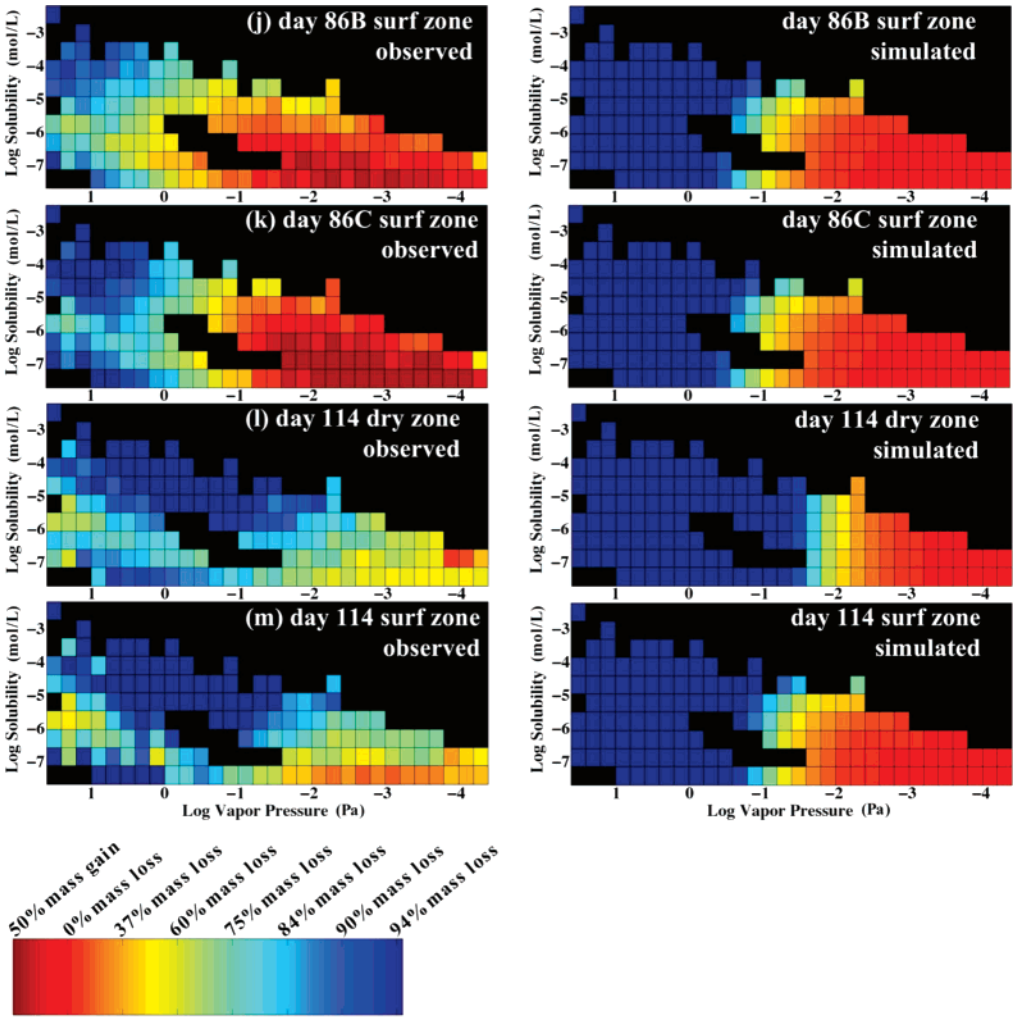

FIGURE 2. Observed and simulated Mass Loss Tables (MLTs) for 13 samples collected from Nyes Neck beach. GC×GC chromatograms were converted into MLTs, in which chromatogram mass losses are distributed with respect to volatility and aqueous solubility. Each MLT cell *i* shows the mass loss, $\ln[M_i(t)/M_i(t_0)]$, of the weathered samples with respect to the fresh oil. Some cells are shaded in black because the original oil did not include compounds that explored this chemical property space. Observed sample trends are compared to simulation predictions. Evaporation systematically removes compounds along the (horizontal) axis of volatility, and dissolution removes compounds along the (vertical) axis of solubility.

time for a given oil loading, and k_i is a PAH-specific loss rate constant. They found that dw/dt was highly anti-correlated ($r^2 = -0.98$) with oil loading. By reanalyzing Short and Heintz's data, we also found a high correlation ($r^2 = 0.98$) between dw/dt and *inverse* oil loading. The latter finding is actually formally exact in eq 5: Short and Heintz's dw/dt corresponds to $D_{water}/(\delta_{water}\delta_{oil})$ in eq 5, and this term is explicitly inverse to oil loading, δ_{oil}. In other words, eq 5 predicts the relationship between dw/dt and inverse oil loading empirically observed in Short and Heintz's data. Taking the interpretation further, the k_i parameter in eq 15 necessarily contains information about $K_{i,w/o}$ in eq 5. Empirically determined values of k_i are consistent with this notion: Short and Heintz reported that $\ln(k_i)$ is anti-correlated to total molecular surface area, therefore $\ln(k_i)$ also correlates with $\ln(K_{i,w/o})$ (*20*). Thus the Short and Heintz empirical PAH loss rate model and associated parameters are partly interpretable in terms of the established transport concepts of eq 5.

Hydrocarbon Mass Apportionments to Air, Water, and Transformations. Mass apportionments, or cumulative losses of hydrocarbon mass to the atmosphere, to the water column, and to transformations, were estimated using the mass transfer model. By projecting simulated MLTs back onto the GC×GC chromatogram of the unweathered oil, mass transfer predictions were applied to the fully resolved mixture. This enabled mass transfer apportionment estimates for any GC×GC-resolved peak (Figure 4). The model predicted that in the surf zone, 31% of the aggregate PAH mass was transferred to the atmosphere (67%) and water column (33%) during the first 114 days (see Supporting Information). However, different PAHs apportioned differently into air and water. For example, surf zone simulations predicted that naphthalene was transferred in equal amounts to atmosphere and ocean (51% to air and 49% to water); C_3-naphthalenes went mostly into the atmosphere (80% to air, 20% to water); and phenanthrene was transmitted predominantly to the ocean (31% to air, 69% to water). Notably, the sequence of conditions (e.g., temperature) affected mass apportionment estimates. Hence, mass transfer apportionment estimates were only distinguishable by explicitly treating mass transfer kinetics. Additionally, apportionment outcomes would differ between arctic and tropical climates. In particular, cold regions will likely experience a higher dissolved hydrocarbon load and greater risk to sensitive aquatic ecosystems. Small PAHs (naphthalenes, phenanthrenes) contribute to the early ecological impact of an oil spill for many aquatic life (*36*), because these compounds are abundant in oils, toxic, and relatively water soluble. Accurate compound apportionments to the water column should improve estimates of water

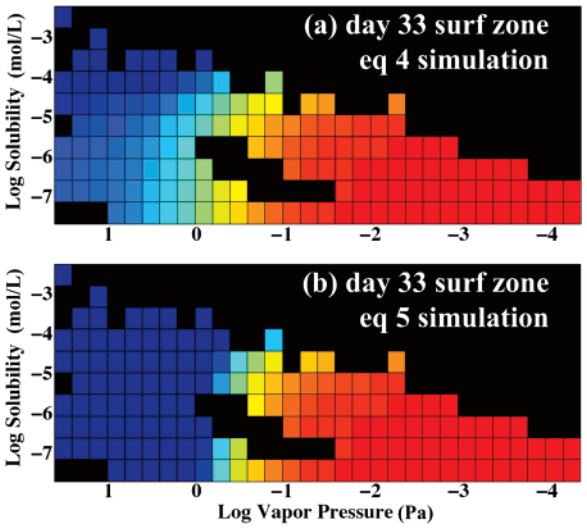

FIGURE 3. Role of oil-side diffusion-limited transport in simulations of the day 33 surf zone. (a) The simulated mass loss tables of the day 33 surf zone composition using eq 4. Evaporation and dissolution are limited by diffusion through the oil phase, and simulations predict a broad mass transfer front. (b) By contrast, if we assumed that oil-side diffusion were negligible (eq 5), the predicted mass transfer signature sharpened into a steeper mass loss front. In other words, oil-side diffusion principally affected (decreased) the mass transfer rates of the highly volatile/soluble compounds.

column concentrations over time, thereby informing assessments of aquatic life exposures to hydrocarbons. In future work, properties relevant to toxicity (i.e., octanol−water partition coefficient) could be mapped (*18*) onto the detailed compositional space of the mixture fraction transferred to the water column.

Discrepancies between simulated and observed hydrocarbon mass losses suggested transformation processes. For example, the observed aggregate PAH mass loss rate was consistent with simulated mass transfer losses during the first 2 months (see Supporting Information). However, in late samples of both the dry zone (days 86 and 114) and surf zone (day 114), simulated mass transfers were insufficient to explain observed losses of aggregate PAH mass, suggesting mass removal by photodegradation and/or biodegradation. Additionally, many samples exhibited excess *n*-alkane losses relative to observed evaporation fronts, indicating biodegradation. In our companion manuscript (*4*), we describe an approach for differentiating the early evaporative and biodegradative removal rates of *n*-alkanes based on observed positions of evaporation fronts in individual samples. Ultimately, the methods developed here should improve accounting of coastal water hydrocarbon loading and advance our understanding of hydrocarbon persistence in weathering oils.

Acknowledgments

We gratefully acknowledge the helpful comments of Dr. Roger Prince and three anonymous reviewers. This work was supported by the NSF (MPS-DRF CHE 0502600 and IIS-0430835) and DOE (DEFG02-06ER15775).

Supporting Information Available

Measured air and water temperatures, and estimated rock temperatures, at Martha's Vineyard Coastal Observatory from April 27 to Aug. 18, 2003; and simulated mass transfers of aggregate PAH mass to the atmosphere and water column compared to observed removal of aggregate PAH mass in Nyes Neck samples. This material is available free of charge via the Internet at http://pubs.acs.org.

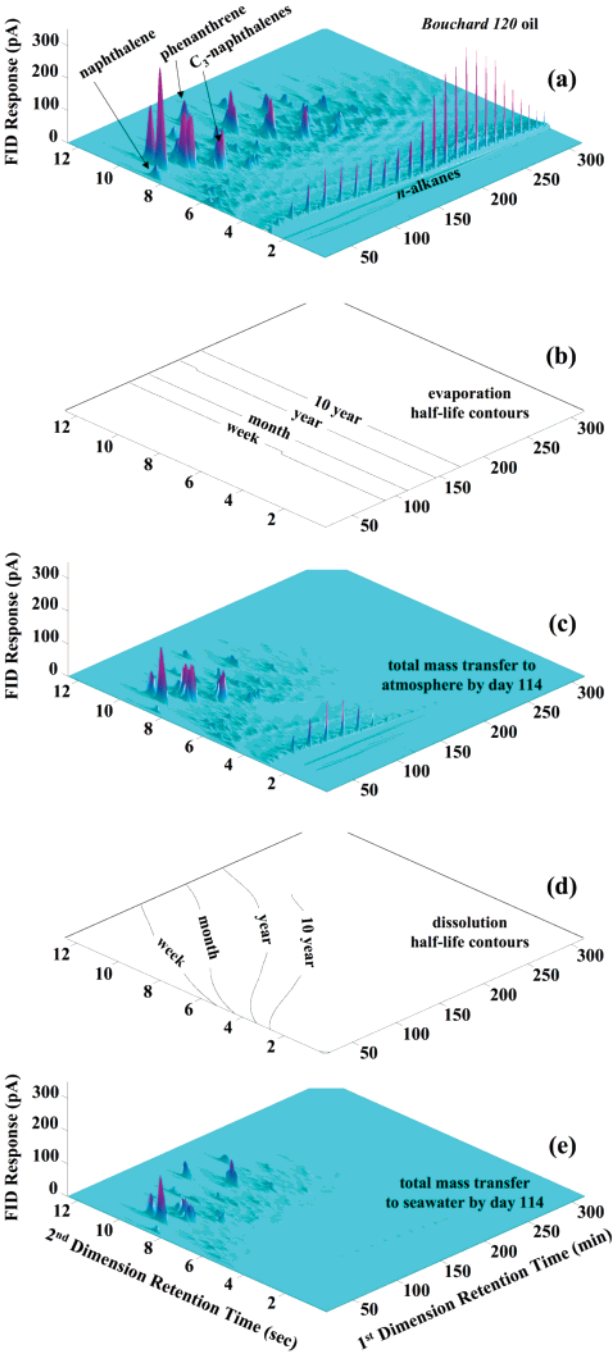

FIGURE 4. Predicted mass transfer half-lives and predicted mass apportionments to air and water, in the surf zone. By projecting model mass transfer predictions back onto the raw chromatogram of the original oil, mass transfer half-lives were mapped onto the GC×GC-resolved compositional space. Quantitative mass apportionments could be estimated for all resolved peaks. (a) GC×GC chromatogram of the original *Bouchard 120* oil. (b) Contours of the evaporation half-life for individual hydrocarbons, based on an instantaneous mass transfer rate calculated with oil thickness = 0.0035 cm and $T = 20$ °C in the surf zone. The evaporation rate depends on T and also accelerates with decreasing oil thickness, so contour values depicted here are high estimates. (c) Total surf zone material that transferred to the atmosphere during the first 114 days of weathering, based on simulations. (d) Contours of the instantaneous dissolution half-life for individual hydrocarbons are projected onto the GC×GC chromatogram, based on oil thickness = 0.0035 cm and surf zone conditions. Since oil thickness decreases over time, depicted contour values are high estimates. (e) Total surf zone mass that transferred to the water column during the first 114 days, based on simulations.

Literature Cited

(1) Nash, R. A. *Memorandum to CG MSO Providence: Gauging reports for the T/B B No 120 oil spill. 29 June*; U.S. Coast Guard, 2004.

(2) NOAA. *Bouchard Barge No. 120 oil spill Pre-Assessment Data Report*; NOAA: Washington, DC, 2005.

(3) Nelson, R. K.; Kile, B. M.; Plata, D. L.; Sylva, S. P.; Xu, L.; Reddy, C. M.; Gaines, R. B.; Frysinger, G. S.; Reichenbach, S. E. Tracking the weathering of an oil spill with comprehensive two-dimensional gas chromatography. *Environ. Forens.* **2006**, *7*, 33−44.

(4) Arey, J. S.; Nelson, R. K.; Reddy, C. M. Disentangling oil weathering using GCxGC. 1. Chromatogram analysis. *Environ. Sci. Technol.* **2007**, *41*, 5738−5746.

(5) Harrison, W.; Winnik, M. A.; Kwong, P. T. Y.; Mackay, D. Crude oil spills. Disappearance of aromatics and aliphatic components from small sea-surface slicks. *Environ. Sci. Technol.* **1975**, *9*, 231−234.

(6) Stiver, W.; Mackay, D. Evaporation rate of spills of hydrocarbons and petroleum mixtures. *Environ. Sci. Technol.* **1984**, *18*, 834−840.

(7) Mackay, D.; Matsugu, R. S. Evaporation rates of liquid hydrocarbon spills on land and water. *Can. J. Chem. Eng.* **1973**, *51*, 434−439.

(8) Liss, P. S.; Slater, P. G. Flux of gases across air-sea interface. *Nature* **1974**, *247*, 181−184.

(9) Goodwin, S. R.; Mackay, D.; Shiu, W. Y. Characterization of the evaporation rates of complex hydrocarbon mixtures under environmental conditions. *Can. J. Chem. Eng.* **1976**, *54*, 290−294.

(10) Drivas, P. J. Calculation of evaporative emissions from multicomponent spills. *Environ. Sci. Technol.* **1982**, *16*, 726−728.

(11) Stiver, W.; Shiu, W. Y.; Mackay, D. Evaporation times and rates of specific hydrocarbons in oil spills. *Environ. Sci. Technol.* **1989**, *23*, 101−105.

(12) Fingas, M. F. A literature review of the physics and predictive modelling of oil spill evaporation. *J. Hazard. Mater.* **1995**, *42*, 157−175.

(13) Sebastiao, P.; Soares, C. G. Modeling the fate of oil spills at sea. *Spill Sci. Technol. Bull.* **1995**, *2*, 121−131.

(14) National Research Council. *Oil in the sea III. Inputs, fates and effects*; National Academy of Sciences: Washington, DC, 2003.

(15) Prince, R. C.; Garrett, R. M.; Bare, R. E.; Grossman, M. J.; Townsend, T.; Suflita, J. M.; Lee, K.; Owens, E. H.; Sergy, G. A.; Braddock, J. F.; Lindstrom, J. E.; Lessard, R. R. The roles of photooxidation and biodegradation in long-term weathering of crude and heavy fuel oils. *Spill Sci. Technol. Bull.* **2003**, *8*, 145−156.

(16) Short, J. W.; Heintz, R. A. Identification of *Exxon Valdez* oil in sediments and tissues from Prince William Sound and the Northwestern Gulf of Alaska based on a PAH weathering model. *Environ. Sci. Technol.* **1997**, *31*, 2375−2384.

(17) Short, J. W. Oil identification based on a goodness-of-fit metric applied to hydrocarbon analysis results. *Environ. Forens.* **2002**, *3*, 349−355.

(18) Arey, J. S.; Nelson, R. K.; Xu, L.; Reddy, C. M. Using comprehensive two-dimensional gas chromatography retention indices to estimate environmental partitioning properties for a complete set of diesel fuel hydrocarbons. *Anal. Chem.* **2005**, *77*, 7172−7182.

(19) Arey, J. S.; Nelson, R. K.; Xu, L.; Reddy, C. M. Using comprehensive two-dimensional gas chromatography retention indices to estimate environmental partitioning properties for a complete set of diesel fuel hydrocarbons, correction. *Anal. Chem.* **2007**, *79*, 4736.

(20) Schwarzenbach, R. P.; Gschwend, P. M.; Imboden, D. M. *Environmental Organic Chemistry*, 2nd ed.; John Wiley & Sons: New York, 2003.

(21) Southworth, G. R.; Herbes, S. E.; Allen, C. P. Evaluating a mass transfer model for the dissolution of organics from oil films into water. *Water Res.* **1983**, *17*, 1647−1651.

(22) Herbes, S. E.; Southworth, G. R.; Allen, C. P. Rates of dissolution of constituent organic contaminants from coal liquefaction oil films into water. *Water Res.* **1983**, *17*, 1639−1646.

(23) Page, C. A.; Bonner, J. S.; Sumner, P. L.; Autenrieth, R. L. Solubility of petroleum hydrocarbons in oil/water systems. *Marine Chem.* **2000**, *70*, 79−87.

(24) Kowert, B. A.; Dang, N. C. Diffusion of dioxygen in *n*-alkanes. *J. Phys. Chem. A* **1999**, *103*, 779−781.

(25) Martin-Alfonso, M. J.; Martinez-Boza, F.; Partal, P.; Gallegos, C. Influence of pressure and temperature on the flow behavior of heavy fuel oils. *Rheol. Acta* **2006**, *45*, 357−365.

(26) Mackay, D.; Buist, I.; Mascarenhas, R.; Petersen, S. *Oil Spill Processes and Models*; Report EE-8; Environment Protection Service: , 1980.

(27) Wolfe, D. A.; Hameedi, M. J.; Galt, J. A.; Watabayashi, G.; Short, J. W.; O'Claire, C.; Rice, S.; Michel, J.; Payne, J. R.; Braddock, J.; Hanna, S.; Sale, D. The fate of the oil spilled from the *Exxon Valdez*. *Environ. Sci. Technol.* **1994**, *28*, 561A−568A.

(28) Fingas, M. F. Studies on the evaporation of crude oil and petroleum products: 1. The relationship between evaporation rate and time. *J. Hazard. Mater.* **1997**, *56*, 227−236.

(29) Michel, J.; Hayes, M. O. Weathering patterns of oil residues eight years after the *Exxon Valdez* oil spill. *Mar. Pollut. Bull.* **1999**, *38*, 855−863.

(30) Wang, Z.; Fingas, M. F.; Owens, E. H.; Sigouin, L.; Brown, C. E. Long-term fate and persistence of the spilled Metula oil in a marine salt marsh environment. Degradation of petroleum biomarkers. *J. Chromatogr. A* **2001**, *926*, 275−290.

(31) Short, J. W.; Irvine, G. V.; Mann, D. H.; Maselko, J. M.; Pella, J. J.; Lindeberg, M. R.; Payne, J. R.; Driskell, W. B.; Rice, S. D. Slightly weathered *Exxon Valdez* oil persists in Gulf of Alaska beach sediments after 16 years. *Environ. Sci. Technol.* **2007**, *41*, 1245−1250.

(32) White, H. K.; Xu, L.; Lima, A. L.; Eglinton, T. I.; Reddy, C. M. Abundance, composition, and vertical transport of PAHs in marsh sediments. *Environ. Sci. Technol.* **2005**, *39*, 8273−8280.

(33) Davis, S. J.; Gibbs, C. F. The effect of weathering on a crude oil residue exposed at sea. *Water Res.* **1975**, *9*, 275−285.

(34) Patton, J. S.; Rigler, M. W.; Boehm, P. D.; Fiest, D. L. Ixtoc 1 oil spill: flaking of surface mousse in the Gulf of Mexico. *Nature* **1981**, *290*, 235−238.

(35) Irvine, G. V.; Mann, D. H.; Short, J. W. Multi-year persistence of oil mousse on high energy beaches distant from the *Exxon Valdez* spill origin. *Mar. Pollut. Bull.* **1999**, *38*, 572−584.

(36) Reddy, C. M.; Quinn, J. G. The *North Cape* oil spill: hydrocarbons in Rhode Island coastal waters and Point Judith Pond. *Mar. Environ. Res.* **2001**, *52*, 445−461.

Received for review January 2, 2007. Revised manuscript received April 24, 2007. Accepted June 3, 2007.

ES070006P